

# Contact angle of water on a model heterogeneous surface. A density functional approach

K. Dąbrowska<sup>1</sup>, O. Pizio <sup>2</sup>, S. Sokołowski <sup>1</sup>

<sup>1</sup> Department of Theoretical Chemistry, Maria Curie-Skłodowska University, Lublin 20-031, Poland, email: stefan.sokolowski@gmail.com

<sup>2</sup> Instituto de Química, Universidad Nacional Autónoma de México, Circuito Exterior, 04510, Cd. de México, México, email: oapizio@gmail.com

Received May 11, 2022, in final form July 13, 2022

We use a density functional approach to calculate the contact angle of the water model on a heterogeneous, graphite-like surface. The surface heterogeneity results from the pre-adsorption of a layer of spherical species. The pre-adsorbed molecules can also be a mixture of molecules of different sizes. The presence of pre-adsorbed layer causes geometrical and energetical heterogeneity of the surfaces. Two cases are considered. The pre-adsorbed molecules can either behave like hard-sphere obstacles, or they can also attract the molecules of water. In the first case, an increase of the amount of pre-adsorbed species leads to an increase of the wetting temperature, but this increase does not depend linearly on the amount of obstacles. In the case of obstacles exerting attractive forces on water molecules, the curves describing the dependence between the amount of pre-adsorbed species and the contact angle can exhibit a maximum. In addition, we have also studied how the pre-adsorbed species influence the local densities of gaseous and liquid phases in contact with a modified solid surface.

**Key words:** *density functional theory, contact angle, heterogeneous surface, water model*

## 1. Introduction

The problem of the influence of surface heterogeneity of solid surfaces on thermodynamic properties of fluid-solid systems has been the subject of intensive research for a long time [1–8]. Usual models of heterogeneous surfaces have been based on distinguishing several kinds of surface active sites. The sites differ by their interaction energy with fluid molecules. The function describing the distribution of sites with the energy is termed “the energy distribution function” and is commonly treated as a characteristic property of a given heterogeneous solid [4].

Different models describing the systems with heterogeneous surfaces have been considered. They can be classified according to the way in which the surface active sites are defined and distributed over a surface. According to the so-called patchwise model, the sites of the same kind are grouped into patches. The patches are geometrically flat, energetically homogeneous and independent of each other. Consequently, thermodynamic properties of a fluid in contact with a patchy heterogeneous solid (e.g., adsorption isotherms) are computed as weighted averages of the relevant properties for homogeneous surfaces with statistical weights resulting from the energy distribution function [2, 4]. However, for several solid surfaces, such as silica gels, aluminum oxides, or active carbons, the patchwise heterogeneous model is unrealistic [6] and considering such systems, the models of random heterogeneous surfaces were introduced [9, 10].

One of the possible statistical-thermodynamic methods of describing the random heterogeneous systems comes from the theory of quenched-annealed systems [11–13]. Although the latter approach is mainly applied in the studies of fluids confined by microporous solids, it can be equally well used for modelling a rough solid surface, or capillaries filled with random matrices [14–16]. The initial flat

surface is covered with a layer of randomly distributed particles, which remain frozen at fixed positions when the fluid enters the system.

The models intermediate between patchwise and random surfaces are patterned surface models. The sites of particular kinds occupy small regions of simple geometrical shape (e.g., stripes, squares, or triangles). These geometrical constructs are ordered into crystalline-like lattices. In contrast to patchwise models, the processes occurring over particular structures are not independent of each other. The thermodynamic properties of fluids in contact with patterned surfaces were studied in several publications, see e.g. [17–21].

The heterogeneity of solid surfaces plays an important role in the adsorption of fluids on solids and in chromatographic processes [22, 23]. Indeed, the presence and specific distribution of adsorption sites on the surfaces can decide about the effectiveness of the separation of fluid mixtures. Furthermore, the surface heterogeneity can strongly influence the surface phase transitions. The studies of the latter problems mainly concern patterned and random surfaces [24–27].

Wetting is an important phenomenon that is common in nature [28]. It is also an essential issue for the design and development of novel substances with desirable surface properties that can be applied in many areas of engineering, chemistry, and biology. One of the most significant ingredients that appear in several processes is water. In particular, the wetting behavior of water on graphite-like substrates was the subject of our recent detailed study [29].

Experimental method for investigating the wetting is usually based on the measurement of the static contact angle,  $\theta$ . A crossover from non-wetting to wetting state takes place if the contact angle changes from a nonzero value to zero [30]. The temperature at which this transition occurs is called the wetting temperature,  $T_w$ . Other experiments rely on the measurements of adsorption isotherms for gas densities up to the saturated vapor density. In the case of first-order wetting transitions, characteristic changes in the course of adsorption isotherms with temperature take place. Namely, at temperatures below  $T_w$ , upon the bulk density approaching the liquid-vapor coexistence, the thickness of the adsorbed film remains finite and small, whereas at higher temperatures, it diverges to infinity [31–33]. Thus, the study of changes of adsorption isotherms allows the determination of  $T_w$ . Note that the adsorption method for the first time permitted to capture the wetting temperature for  $^4\text{He}$  on cesium [34].

Of course, the value of the static contact angle,  $\theta$ , depends on the surface heterogeneity. However, there is no general approach that would describe  $\theta$  in terms of parameters characterizing the surface heterogeneity. Although several attempts to elucidate the effects of surface heterogeneity on the values of  $\theta$  were undertaken, but they concerned specific surface models. For patchy heterogeneous surfaces, Cassie and Baxter [35] proposed an expression relating the contact angle to the energy distribution function. Another attempt was proposed by Wenzel [36] for macroscopically rough surfaces. Both Cassie-Baxter and Wenzel approaches were next applied and verified for numerous systems, cf. reference [37] and the references quoted therein. The Cassie-Baxter and Wenzel equations can be used if the patches are big enough, i.e., if their size is much larger than the range of capillary forces. We would like to stress that the Cassie-Baxter equation for the contact angle is familiar [38] to the so-called integral equation for the adsorption isotherm, [4]. Recent studies, however, concentrated on the description of patterned surfaces composed of alternately arranged hydrophilic and hydrophobic regions [39–45].

One of the methods [46, 47] for modifying the surface properties of solids relies on pre-adsorption of some selected species on bare surfaces, e.g., chain molecules (oligomers and polymers). This method has found particularly important applications in developing novel chromatographic column packing with the required properties [48, 49]. The grafted chains have also a significant impact on the surface phase transitions, such as wetting, layering, and capillary condensation in confined fluids [50–52]. As our recent study indicated, the grafted chains are capable not only of quantitatively but also qualitatively influencing the topology of the surface phase diagrams [53].

Theoretical methods for the description of surface phase transitions are mainly based on the density functional approaches [54]. Density functional theories can be also employed to the systems with surfaces modified by chemically bonded spherical molecules. Therefore, in this work, we propose a density functional method to study the changes of static contact angle with the changes of the adsorbing surface amount and size of pre-adsorbed spherical molecules.

The fluid-fluid interaction is selected to mimic the interaction between a pair of water molecules. Water belongs to the class of associating fluids and the formation of intermolecular hydrogen (associative)

bonds should be taken into account in the model. However, the application of contemporary force fields for water with site-site electrostatic forces [55] would be computationally prohibitive within the density functional approaches. Therefore, we use the potential resulting from the statistical association fluid theory (SAFT), [56, 57] with the parameters proposed by Clark et al. [58]. This model is not only one of the most accurate in terms of evaluating the liquid-vapor phase diagram, but it also correctly predicts the temperature dependence of the surface tension [58, 59].

Water molecules are in contact with a modified surface of graphite. Similarly to our previous work [29], the Lennard-Jones 10-4-3 function [60] is used to describe the interaction of a water particle with a bare graphite surface. The surface of graphite is covered with a layer of pre-adsorbed spherical molecules. The pre-adsorbed layer can be either one- or many-component and we consider the cases of purely repulsive and repulsive and attractive interactions with water molecules. The values of the equilibrium contact angle are then calculated from the density functional theory. The theory used for us is a modification of the approach for grafted chain molecules [15, 16]. The pre-adsorbed layer creates both geometrical and energetic heterogeneity of an adsorbing surface. However, we should also mention here that there exist alternative density functional approaches proposed by Aslymov and co-workers [61, 62] and by Zhou [63], based on the development of an appropriate expression for the “effective” fluid-solid that takes into accounts the surface roughness. This effective potential is then used as an external potential field in the classical density functional treatment. Our approach, however, leads to modifications of the expressions for the system free energy.

The paper is arranged as follows. In the next section we briefly outline the details of the model and the interaction potentials. Then, we describe the basic points of the density functional theory and the method for the evaluation of the values of the contact angle. Section 3 presents the results obtained for the pre-adsorbed layer formed by one-component layer of hard spheres (obstacles), built of a binary mixture of obstacles, and, finally, we consider the case of pre-adsorbed particles interacting via repulsive and attractive forces. The last section concludes the obtained theoretical data.

## 2. Model and theory

### 2.1. Interaction potentials

According to the model developed by Chapman, Gubbins, and Jackson [64, 65], each water molecule possesses four associative sites  $\Gamma = \{A, B, C, D\}$ , located at the vertices of tetrahedron inscribed into a spherical core. The interaction energy between the molecules  $i = 1, 2$  depends on the center-to-center distance,  $r_{12} = |\mathbf{r}_{12}|$ , and on orientations of both molecules,  $\omega_i$ ,

$$u(12) = u_{ff}(r_{12}) + \sum_{\alpha \in \Gamma} \sum_{\beta \in \Gamma} u_{\alpha\beta}(\mathbf{r}_{\alpha\beta}). \quad (2.1)$$

The site-site vectors,  $\mathbf{r}_{\alpha\beta}$ , are  $\mathbf{r}_{\alpha\beta} = \mathbf{r}_{12} + \mathbf{d}_\alpha(\omega_1) - \mathbf{d}_\beta(\omega_2)$ , where  $\mathbf{d}_i(\omega_i)$  is the vector connecting the site  $i$  on molecule  $i$  with its center (see also figure 1 of reference [64]). Only the site-site association AC, BC, AD, and BD is allowed, and all association energies are equal. The associative interaction between the sites is

$$u_{\alpha\beta}(\mathbf{r}_{\alpha\beta}) = \begin{cases} -\varepsilon_{\text{as}}, & 0 < |\mathbf{r}_{\alpha\beta}| \leq r_c, \\ 0, & |\mathbf{r}_{\alpha\beta}| > r_c, \end{cases} \quad (2.2)$$

where  $\varepsilon_{\text{as}}$  is the depth and  $r_c$  is the cut-off range of the associative interaction.

The non-associative part of the pair potential,  $u_{ff}(r)$ , is described by a square-well potential

$$u_{ff}(r) = u_{\text{hs},ff}(r) + u_{\text{att},ff}(r), \quad (2.3)$$

where  $u_{\text{hs},ff}(r)$  and  $u_{\text{att},ff}(r)$  are, respectively, the hard-sphere (hs) and attractive (att) parts of the potential,

$$u_{\text{hs},ff}(r) = \begin{cases} \infty, & r < \sigma, \\ 0, & r \geq \sigma, \end{cases} \quad (2.4)$$

and

$$u_{\text{att},ff}(r) = \begin{cases} 0, & r < \sigma, \\ \varepsilon, & \sigma \leq r < \lambda_{ff}\sigma, \\ 0, & r \geq \lambda_{ff}\sigma. \end{cases} \quad (2.5)$$

In the above,  $\sigma$ ,  $\varepsilon$  and  $\lambda_{ff}$  are the diameter, the depth and the range of the non-associative water-water potential, respectively.

The parameters for the W1 model of Clark et al. [58] are collected in table 1.

**Table 1.** The parameters of the W1 water-water model potential from reference [58].

Model	$\sigma$ (nm)	$\varepsilon/k$ (K)	$\lambda$	$r_c$ (nm)	$\varepsilon_{\text{as}}/k$ (K)	$ \mathbf{d}_i /\sigma$
W1	0.303420	250.000	1.78890	0.210822	1400.00	0.25

Water molecules are in contact with a modified surface. The initial, non-modified surface is assumed to be graphite-like. The adsorbing potential,  $v(z)$ , exerted on a fluid particle is then given by the potential developed by Steele [60].

$$v(z) = \varepsilon_{fw} \left[ \frac{2}{5} \left( \frac{\sigma_{fw}}{z} \right)^{10} - \left( \frac{\sigma_{fw}}{z} \right)^4 - \frac{\sigma_{fw}^4}{3\Delta(z + 0.61\Delta)^3} \right], \quad (2.6)$$

where  $\varepsilon_{fw}$  and  $\sigma_{fw}$  are the energy and the size parameters, respectively. The interlayer spacing of the graphite planes equals  $\Delta = 0.335$  nm. The values of  $\sigma_{fw}$  and  $\varepsilon_{fw}$  follow from Lorentz-Berthelot mixing rules. Thus, [29],  $\sigma_{fw}/\sigma = 1.06028$  and  $\varepsilon_{fw}/\varepsilon = 8.311$ . Our calculations were also carried out for  $\varepsilon_{fw}/\varepsilon = 7$  and 9.5. The potential of Steele was widely used with success in the theory of adsorption of fluids on graphite [29, 66]. A comprehensive discussion of this potential was provided by Zhao and Johnson [67].

The inhomogeneity of the surface results from its chemical modification. According to our model, the modification means the “sticking” (tethering) of spherical particles of diameters  $\sigma_i$  at the distance  $\sigma_i/2$  from the surface. For the surface at  $z = 0$ , the potential that leads to the tethering of molecules reads

$$\exp[-v_i^{(1)}(z)/kT] = \delta(z - \sigma_i/2), \quad (2.7)$$

where  $\delta$  denotes the Dirac function.

The amount of tethered species  $i$  is controlled by the parameter  $R_{ci}$  that gives the total surface density of pre-adsorbed species. (In the case of one-component pre-adsorbed layer, we drop the subscript  $i$  and use the symbol  $R_c$ .)

Similarly to the case of non-associative water-water interaction, the interaction of water molecules with pre-adsorbed species,  $u_{fi}(r) = u_{\text{hs},fi}(r) + u_{\text{att},fi}(r)$ , is described by the square well potential

$$u_{\text{hs},fi}(r) = \begin{cases} \infty, & r < \sigma_{fi}, \\ 0, & r \geq \sigma_{fi}, \end{cases} \quad (2.8)$$

and

$$u_{\text{att},fi}(r) = \begin{cases} 0, & r < \sigma_{fi}, \\ \varepsilon_{fi}, & \sigma_{fi} \leq r < \lambda_{fi}\sigma_{fi}, \\ 0, & r \geq \lambda_{fi}\sigma_{fi}. \end{cases} \quad (2.9)$$

The interactions between pre-adsorbed species, however, are assumed to be of hard-sphere type with the cross size parameters equal to  $(\sigma_i + \sigma_j)/2$ .

## 2.2. Density functional theory

The system is studied using a version of the density functional theory (DF), described already in detail in references [15, 16]. To avoid unnecessary repetitions, we recall only basic equations.

The symbols  $\rho(\mathbf{r})$  and  $\rho_i(\mathbf{r})$  denote the local density of water-like molecules and of tethered particles of the kind  $i$ . As usual, we start with defining the excess surface free energy (the grand canonical potential) as a functional of the local densities

$$\Omega = F[\rho(\mathbf{r}), \{\rho_i(\mathbf{r})\}] + \sum_{\{i\}} \int d\mathbf{r} \rho_i v_i(z) + \int d\mathbf{r} \rho(\mathbf{r}) [v(z) - \mu], \quad (2.10)$$

where  $\mu$  is the chemical potential of water and  $F[\rho(\mathbf{r}), \{\rho_i(\mathbf{r})\}]$ . At fixed values of temperature and the amount of pre-adsorbed species of all kinds,  $\Omega$  is a function of  $\mu$ , or, alternatively, the bulk density of water,  $\rho_b$ ,  $\Omega = \Omega(\rho_b)$ .

The free energy functional is considered as the sum of an ideal term,  $F_{\text{id}}[\rho(\mathbf{r}), \{\rho_i(\mathbf{r})\}]$ , the hard-sphere functional  $F_{\text{hs}}[\rho(\mathbf{r}), \{\rho_i(\mathbf{r})\}]$ , the functional arising from attractive interparticle forces,  $F_{\text{att}}[\rho(\mathbf{r}), \{\rho_i(\mathbf{r})\}]$  and the part due to the formation of associative bonds,  $F_{\text{as}}[\rho(\mathbf{r}), \{\rho_i(\mathbf{r})\}]$ .

$$F[\rho(\mathbf{r}), \{\rho_i(\mathbf{r})\}] = F_{\text{id}}[\rho(\mathbf{r})] F_{\text{hs}}[\rho(\mathbf{r}), \{\rho_i(\mathbf{r})\}] + F_{\text{att}}[\rho(\mathbf{r}), \{\rho_i(\mathbf{r})\}] + F_{\text{as}}[\rho(\mathbf{r}), \{\rho_i(\mathbf{r})\}]. \quad (2.11)$$

The ideal term is known exactly

$$F_{\text{id}}/kT = \int d\mathbf{r} \rho(\mathbf{r}) [\ln \rho(\mathbf{r}) - 1]. \quad (2.12)$$

The hard-sphere functional is evaluated according to the theory originally developed by Rosenfeld and modified in [68]. It requires the knowledge of four scalar  $[n^{(I)}(\mathbf{r}), I = 0, 1, 2, 3]$  and two vector  $[n^{(VI)}(\mathbf{r}), I = 1, 2]$  averaged densities

$$n^{(L)}(\mathbf{r}) = \int d\mathbf{r}' \rho(\mathbf{r}') w^{(L)}(|\mathbf{r} - \mathbf{r}'|) + \sum_{\{i\}} \int d\mathbf{r}' \rho_i(\mathbf{r}') w_i^{(L)}(|\mathbf{r} - \mathbf{r}'|), \quad (2.13)$$

where  $L = 0, 1, 2, 3, VI, V2$  and  $w^{(L)}(|\mathbf{r} - \mathbf{r}'|)$  are the weight functions, see equations (11)–(14) of reference [68]. However, the explicit equations for the hard-sphere free energy is given by equation (11) of [15].

The attractive forces contribution results from the mean-field approximation. According to the introduced model, the pre-adsorbed molecules do not interact with each other by attractive forces. Thus,

$$F_{\text{att}}[\rho(\mathbf{r}), \{\rho_i(\mathbf{r})\}] = \frac{1}{2} \int \int d\mathbf{r} d\mathbf{r}' \rho(\mathbf{r}') \rho(\mathbf{r}) u_{\text{att},ff}(|\mathbf{r}' - \mathbf{r}|) + \sum_{\{i\}} \int \int d\mathbf{r} d\mathbf{r}' \rho(\mathbf{r}') \rho_i(\mathbf{r}) u_{\text{att},fi}(|\mathbf{r}' - \mathbf{r}|). \quad (2.14)$$

Finally, the contribution arising from the formation of associative bonds between water molecules follows from the application of the first-order thermodynamic theory of Wertheim (TPT1). The TPT1 contribution to the free energy is expressed in terms of the fraction of molecules not bonded at a given site  $\chi(\mathbf{r})$ , which represents the statistical mechanical analogue of the mass action law. The expression used by us for  $F_{\text{as}}[\rho(\mathbf{r}), \{\rho_i(\mathbf{r})\}]$  reads [52]

$$F_{\text{as}}[\rho] = 4 \int d\mathbf{r} n_0(\mathbf{r}) \zeta(\mathbf{r}) \left\{ \ln \chi(\mathbf{r}) - \frac{1}{2} [\chi(\mathbf{r}) - 1] \right\}. \quad (2.15)$$

All the details and the definition of the functions  $\zeta(\mathbf{r})$  and  $\chi(\mathbf{r})$  are given in previous works [52, 69]. We omit here their explicit expressions to avoid unnecessary repetitions.

The density profile  $\rho(\mathbf{r})$  results from the Euler-Lagrange equation,

$$\delta\Omega/\delta\rho(\mathbf{r}) = 0. \quad (2.16)$$

The density profiles of pre-adsorbed species, however, are fixed by the external potential, equation (2.7), and the assumption about constancy of pre-adsorbed particles of the kind  $i$ . This means that

$$\int dz \rho_i(z) = R_{ci}, \quad (2.17)$$

i.e.,  $\rho_i(z) = R_{ci} \delta(z - \sigma_i/2)$ .

If the external field depends on the distance perpendicular to the solid surface only, as in equation (2.6), then the local density is one-dimensional as well, i.e.  $\rho(\mathbf{r}) \equiv \rho(z)$ . The Euler-Lagrange equation for the density profile can be solved using different numerical procedures, see e.g., [70] and references therein. In our calculations, we used the classical Picard iteration method.

### 2.3. Contact angle

The criterion for wetting the surface by a liquid is usually derived from the classical Young's equation that expresses the force balance at a three-phase contact between a liquid drop ( $l$ ), a solid surface ( $s$ ) and a gas phase ( $g$ ), in terms of the contact angle,  $\theta$  [30, 31] as

$$\gamma_g - \gamma_l = \gamma \cos \theta, \quad (2.18)$$

where  $\gamma_\kappa = \Delta\Omega_\kappa/A$  is the interfacial tension at gas-solid ( $\kappa = g$ ) and at liquid-solid ( $\kappa = l$ ) interface,  $A$  is the interfacial surface area,  $\Delta\Omega_g = \Omega(\rho_{bg}) - \Omega_b(\rho_{bg})$  and  $\Delta\Omega_l = \Omega(\rho_{bl}) - \Omega_b(\rho_{bl})$  are the excess grand thermodynamic potentials for the gas-solid and for the liquid-solid interfaces calculated for the bulk densities  $\rho_{bg}$  and  $\rho_{bl}$  corresponding to the densities of coexisting gaseous and liquid bulk phases. Next,  $\Omega_b$  is the bulk grand thermodynamic potential at the bulk liquid-vapor coexistence and  $\gamma$  is the gas-liquid interfacial tension (the surface tension).

The Young equation is an approximation to reality [71] as it neglects the effect of the line tension at a three-phase contact. The wetting temperature,  $T_w$ , is determined as the highest temperature at which the ratio  $(\gamma_g - \gamma_l)/\gamma$  becomes zero for the first time. At temperatures  $T \geq T_w$ , the liquid drop completely spreads across the surface.

The applications of equation (2.18) requires the knowledge of the values of the surface tension,  $\gamma$ . In order to evaluate them, one needs to calculate the changes of the local density across the interface between semi-infinite slab of a liquid and a semi-infinite slab of a gas. This is done by removing the solid wall and setting the boundary conditions to  $\rho(z = -\infty) = \rho_l$  and  $\rho(z = \infty) = \rho_g$ , using the procedure described in detail in reference [72].

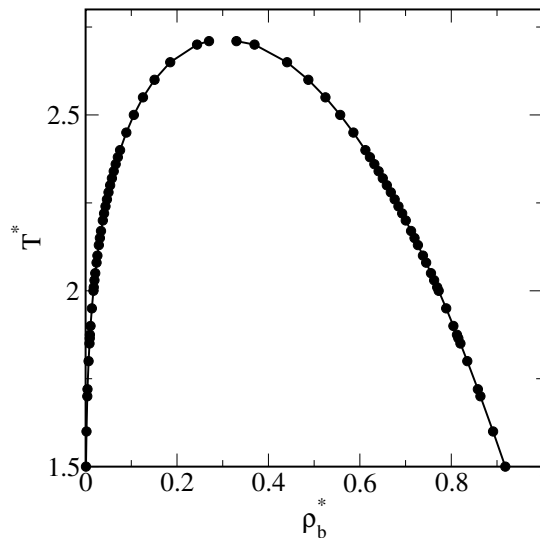


**Figure 1.** Bulk liquid-vapor phase diagram in the temperature-density plane for the model W1 of water.

### 3. Results and discussion

All variables below are expressed in reduced units. The reduced temperature, reduced distance, reduced diameter and a reduced amount of pre-adsorbed particles, as well as a reduced local and bulk density are  $T^* = kT/\varepsilon$ ,  $z^* = z/\sigma$ ,  $\sigma_i^* = \sigma_i/\sigma$ ,  $R_c^* = R_c\sigma^2$  and  $\rho^*(z) = \rho(z)\sigma^3$ , and  $\rho_b^* = \rho_b\sigma^3$ , respectively.

Evaluation of the contact angles requires the knowledge of two bulk densities at the gas-liquid coexistence. The calculation of the bulk phase diagram was self-consistently carried out using the bulk version of the density functional theory [29], and the obtained phase diagram is given in figure 1. Similarly, the values of the liquid-vapor surface tension were obtained using the density functional method and all the details of these calculations are outlined in [29].

We have already noted that similarly to our previous works [29, 53], the calculations were carried out for the W1 model of Clark et al. [58]. The parameters of this model were selected so as to reproduce the experimental bulk liquid-gas phase diagram. Therefore, the agreement between theoretical and experimental bulk dew and bubble densities is quite good, in general. However, the data fitting of Clark was at temperatures lower than the bulk critical temperature. Thus, some deviations can appear between bulk theoretical and experimental data within the temperatures range in the vicinity of the critical temperature. When assessing the results presented below, we should remember that a lower accuracy of the bulk system description for temperatures close to the critical temperature may have an impact on the predictions of the applied theory. Note that the bulk critical temperature resulting from our approach [29, 73],  $T_c^* \approx 2.715$ , is in a reasonable agreement with experiment.

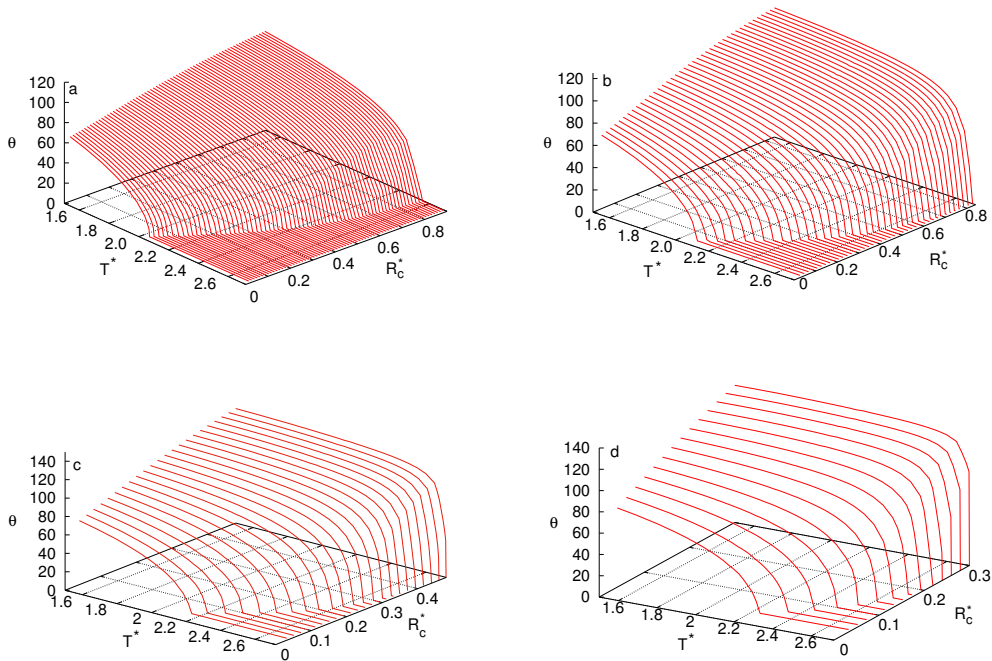


**Figure 2.** (Colour online) The dependencies of the static contact angle  $\theta$  on temperature and the amount of pre-adsorbed particles of the diameter  $\sigma_1 = 0.8$  (part a),  $\sigma_1 = 1$  (part b),  $\sigma_1 = 1.2$  (part c) and  $\sigma_1 = 1.4$  (part d). The calculations are for  $\varepsilon_{fw}^* = 8.311$ .

The first series of calculations were carried out for the surface covered by a one-component layer of hard-sphere obstacles, i.e., the interaction of a pre-adsorbed molecule with water molecules was of hard-sphere type. Four sizes of pre-adsorbed particles were studied:  $\sigma_1^* = 0.8, 1, 1.2, \text{ and } 1.4$ .

The pre-adsorbed molecules block the access to the surface of the adsorbate molecules. As a consequence, the effective (i.e., averaged over the entire surface) surface-water interactions become weaker. Since the wetting of a solid surface results from a balance of solid-fluid and fluid-fluid interactions, one can expect an increase of the wetting temperature with the surface density  $R_c^*$  of pre-adsorbed species.

In figure 2 we show three dimensional plots illustrating the dependence of the contact angle on temperature and on  $R_c^*$ . The calculations are for  $\varepsilon_{fw}^* = 8.311$ .

For  $\sigma_1^* = 1.4$  (figure 2 d), the wetting occurs only for surface densities  $R_c^* \lesssim 0.25$  (or, for  $R_c \sigma_1^2 \lesssim 0.49$ ). The close-packed hexagonal surface coverage corresponds to the surface density  $R_{cp}^* \sigma_1^2 = 2/\sqrt{3}$ . Therefore, the covering of approximately 40% of the surface by hard obstacles of the diameter  $\sigma_1^* = 1.4$  suffices to prohibit the wetting at all temperatures  $T^* < T_c^*$ . In the case of the particles of diameter  $\sigma_1^* = 1$  (figure 2 b), the covering of the surface that inhibits the wetting is higher and equals approximately  $R_c \sigma_1^2 \approx 0.82$ , which corresponds to 71% of the close-packed coverage. Of course, the higher efficiency of larger hard particles in retarding the wetting is connected with stronger lowering of the effective water-surface interactions by obstacles of larger size.

At low temperatures, the plots of  $\theta(T)$  exhibit a plateau. This type of behavior is more evident for larger obstacles and at higher values of  $R_c^*$ . In other words, with an increasing  $R_c^*$ , the surface becomes more hydrophobic for a wider range of temperatures. We checked that at  $T^* = 1.5$ , the contact angle for the surface covered with the close-packed hexagonal layer of particles of  $\sigma^* = 1$  is  $\theta \approx 110^\circ$ , while for  $\sigma_1^* = 1.4$  it equals  $\approx 130^\circ$ .

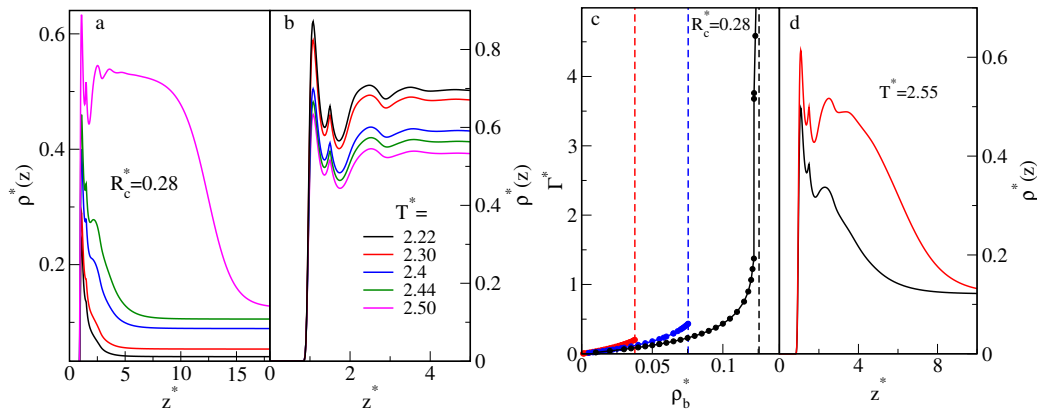


**Figure 3.** (Colour online) Parts a and b. Local density profiles at different temperatures for bulk density marginally lower than bulk dew density (part a) and marginally higher than the bubble density (part b). The temperatures are given in part b. Part c. Adsorption isotherm from gaseous phase at  $T^* = 2.2$  (red lines), 2.4 (blue lines), and 2.55 (black lines). Vertical dashed lines mark the bulk dew densities. Part d. Local densities for coexisting thin (black) and thick (red) adsorbed films at  $T^* = 2.55$  and for the bulk density  $\rho_b^* = 0.1220$  (the bulk dew density equals  $\approx 0.1256$ ). All calculations are for  $\sigma^* = 1$ ,  $R_c^* = 0.28$  and for  $\varepsilon_{fw}^* = 8.311$ .

Calculations of the contact angles from equation (2.18) require the knowledge of the local densities of the systems for bulk densities equal to the densities of coexisting liquid and gaseous phases. Figures 3 a and 3 b show the density profiles of water at bulk densities marginally lower (part a) and marginally higher (part b) than the densities at the bulk coexistence. The calculations are for  $\sigma_1^* = 1$  and  $R_c^* = 0.28$ . Up to the temperature  $T_c^* = 2.44$  only a thin film formation is observed for adsorption from the gaseous phase. At  $T_c^* = 2.5$ , however, a thick film is formed and its thickness diverges as the bulk density approaches  $\rho_{bg}^*$ . The crossover between thin and thick film behavior is at  $T_w^* = 2.445$ . At the same temperature, the value of the contact angle becomes zero. This indicates a consistency of the values of the wetting temperature obtained from the Young equation and from the adsorption study.

In figures 3 c and 3 d we plot the adsorption isotherms at  $T^* = 2.2$ , 2.4 and  $T^* = 2.55$  (part c), as well as the density profiles (part d) at  $T^* = 2.55$ . Vertical dashed lines in part c indicate the bulk



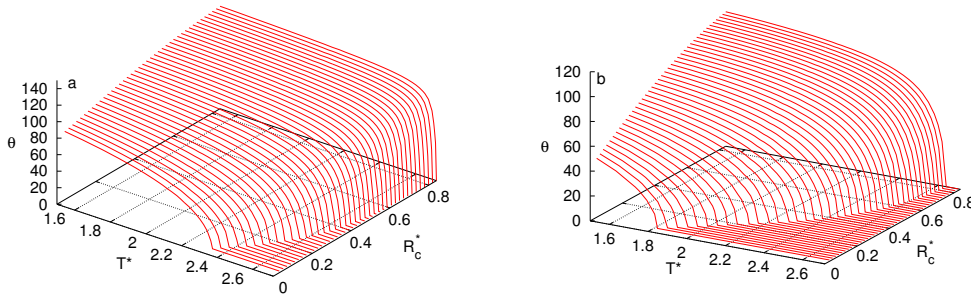


**Figure 4.** (Colour online) The dependencies of the static contact angle  $\theta$  on temperature and the amount of pre-adsorbed particles of the diameter  $\sigma_1^* = 1$  and for  $\varepsilon_{fw}^* = 7$  (part a) and  $\varepsilon_{fw}^* = 9.5$  (part b).

densities of gas coexisting with a liquid. At two lower temperatures, the isotherm remains small up to the bulk liquid-vapor coexistence. At  $T^* = 2.55$ , however, the prewetting jump on the adsorption isotherm appears at  $\rho_b^* = 0.1220$ . The local densities in part d show the profiles just before and after the prewetting jump. According to our estimation, for the system under study, the prewetting jump ends at the critical prewetting temperature,  $T_{cp}^* \approx 2.61$ . Although we did not conduct detailed studies of the prewetting phase transition, the obtained results indicate that for all systems under study, if the prewetting exists, it is a first-order phase transition [29, 31, 33].

In the case of non-modified surfaces, the wetting temperature depends on the depth of the water-surface potential [equation (2.6)],  $\varepsilon_{fw}^*$ . If  $\varepsilon_{fw}^*$  increases, the wetting temperature decreases. A similar behavior was found for surfaces modified with hard obstacles, which is illustrated in figure 4. The calculations were carried out for  $\sigma_1^* = 1$ . Part a shows the dependence of  $\theta$  on temperature and  $R_c^*$  for  $\varepsilon_{fw}^* = 7$ , and part b — for  $\varepsilon_{fw}^* = 9.5$ . Note that according to the results of our previous work for non-modified surfaces [29], the wetting temperature was  $T_w^c = 2.29$  for  $\varepsilon_{fw}^* = 7$  and  $T_w^c = 1.76$  for  $\varepsilon_{fw}^* = 9.5$ .

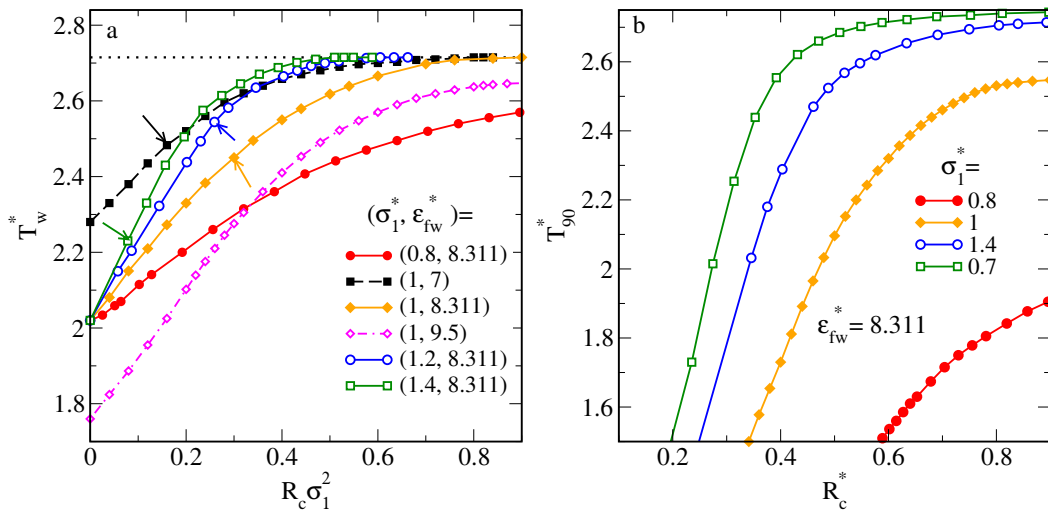


**Figure 5.** (Colour online) The dependence of  $T_w^*$  (part a) and  $T_{90}^*$  (part b) on the amount of pre-adsorbed particles for different values of  $\sigma_1^* = 1$  and  $\varepsilon_{fw}^*$ , given in the figure. The dotted line in part a denotes the bulk critical temperature. The meaning of arrows is explained in the text. We stress that the scale of the abscissa in part a is  $R_c \sigma_1^2$ , while in part b we use the reduced values of  $R_c^*$ .

The presence of hard obstacles leads to the effect of a further lowering of the effective adsorbing potential and thus to an increase of the wetting temperature. For a weakly adsorbing surface,  $\varepsilon_{fw}^* = 7$ , and for high surface density of pre-adsorbed particles,  $R_c^* \gtrsim 0.7$ , the wetting transition disappears for all temperatures  $T^* < T_c^*$ . By contrast, for  $\varepsilon_{fw}^* = 9.5$ , the wetting transition was observed for all investigated values of  $R_c^*$ .

Summary of our calculations for the surfaces covered with hard-sphere obstacles is given in figure 5. Part a presents the dependence of the wetting temperature on  $R_c^*$  for different sizes of obstacles and for three values of  $\varepsilon_{fw}^*$ . In the experimental studies of wetting, the temperature at which the contact angle becomes equal to  $90^\circ$  is important since experimental works usually classify the surfaces with the contact angle  $\theta > 90^\circ$  as hydrophobic and the surfaces with  $\theta < 90^\circ$  — as hydrophilic. The temperature abbreviated as  $T_{90}^*$ , separates these two regimes. We emphasize that in the case of capillaries with hydrophobic walls, the meniscus of fluid inside the pores is concave, while it is convex for hydrophilic walls. The relationship of  $T_{90}^*$  on the surface coverage and the size of obstacles is presented in figure 5 b.

Two groups of the curves can be distinguished in figure 5 a. The first group is at a constant value of  $\varepsilon_{fw}^* = 8.311$  and illustrates the effect of the size of obstacles on the wetting temperature. All three these curves originate at  $(R_c^* = 0, T_c^* = 2.02)$ , i.e., at the wetting temperature for a non-modified surface. The second group of the curves is for the fixed value of  $\sigma_1^* = 1$  and for three values of  $\varepsilon_{fw}^* = 7, 8.311$  and  $9.5$ . Of course, in this case, the wetting temperature for different non-modified surfaces is different.

All the curves in figure 5 exhibit non-linear behavior. Thus their shape contradicts the predictions by Cassie and Baxter [35] theory. In the case of four curves (marked by the arrows in figure 5 a), there exist the values of the surface coverage  $R_w \sigma_1^2$  at which the wetting temperature becomes equal to the bulk critical temperature. For the coverages  $R_c \sigma_1^2 > R_w \sigma_1^2$ , the wetting transition is suppressed for all temperatures up to the bulk critical temperature. The value of  $R_w \sigma_1^2$  is lower for higher  $\sigma_1^*$  and for lower  $\varepsilon_{gs}^*$ . For  $\sigma_1^* = 0.8$  and  $\varepsilon_{fw}^* = 8.311$ , as well as for  $\sigma_1^* = 1$  and  $\varepsilon_{fw}^* = 9.5$ , the wetting transition occurs for all surface coverages  $R_c^*$ .

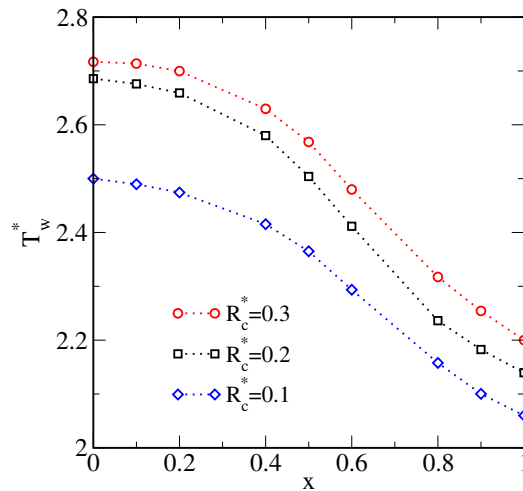


**Figure 6.** (Colour online) The dependencies of  $T_w^*$  on the composition  $x = R_{c1}^* / (R_{c1}^* + R_{c2}^*)$  of a binary pre-adsorbed phase of hard-particles of the diameter  $\sigma_1^* = 0.8$  and  $\sigma_2^* = 1.4$ . The calculations are for fixed values of  $R_c^* = R_{c1}^* + R_{c2}^*$  given in the figure.

We also performed the calculation of the contact angles for two-component pre-adsorbed layers consisting of hard-sphere obstacles of the diameters  $\sigma_1^* = 0.8$  and  $\sigma_2^* = 1.4$ . Figure 6 shows the dependence of the wetting temperature on the composition of the obstacles,  $x = R_{c1}^* / (R_{c1}^* + R_{c2}^*)$ . The displayed results were obtained at three selected constant values of the total two-dimensional density  $R_c^* = R_{c1}^* + R_{c2}^*$ . Of course, for  $x = 0$  and for  $x = 1$ , the wetting temperatures are equal to those of one-component layers consisting of spheres of the diameter  $\sigma_1^* = 1.4$  and  $0.8$ , respectively. Again,

contrary to the Cassie and Baxter [35] theory, the curves in figure 6 are non-linear.

The second series of calculations were for a layer of pre-adsorbed molecules interacting with water molecules via attractive forces. The interactions between pre-adsorbed particles were still of hard-sphere type. We assumed the diameter of pre-adsorbed species to be the same as the diameter of water species,  $\sigma_1^* = 1$ . The energy parameter of the potential of equation (2.9) was treated as a free parameter,  $\varepsilon_{f1}^* = \varepsilon_{f1}/\varepsilon$ .

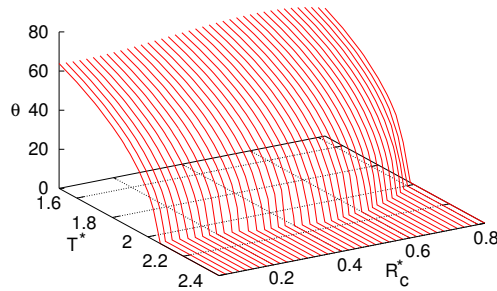


**Figure 7.** (Colour online) The dependence of  $\theta$  on  $T^*$  and  $R_c^*$  for the system with attractive interactions between water and pre-adsorbed species. Calculations are for  $\sigma_1^* = 1$  and  $\varepsilon_{f1}^* = 0.4$ .

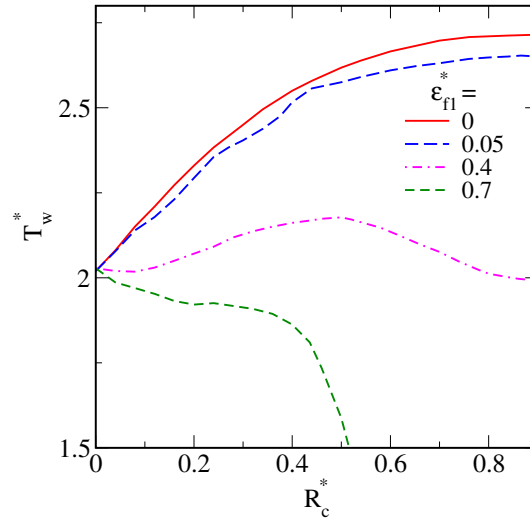
The presence of species attracting the water molecules leads to two opposite effects. The first one results from blocking the access of water molecules to the surface. Consequently, the effective water-surface interactions are lower, and the wetting temperature would increase. However, the pre-adsorbed molecules also exert attractive forces on water molecules. If the second effect prevails, the wetting temperature would decrease. Competition between these two factors can lead to a dependence of the wetting temperature on  $R_c^*$  that could exhibit an extreme.

Figure 7 shows a three-dimensional plot of the dependence of  $\theta$  on temperature and  $R_c^*$ . The presented results are for  $\varepsilon_{f1}^* = 0.4$ . At very low values of  $R_c^*$ , a small decrease of the wetting temperature compared to the bare substrate occurs. It means that for small  $R_c^*$ , the increase of effective attraction between fluid molecules and the modified solid is more important than the effect due to the blocking of the surface. At still higher values of  $R_c^*$  the wetting temperature starts to increase and attains its maximum value for  $R_c^* \approx 0.51$ . Within this region of surface coverages, the blocking effect plays a dominant role. A further increase of  $R_c^*$  leads to the lowering of the wetting temperature.

A comparison of the changes in the wetting temperature with the two-dimensional the density of pre-adsorbed species and with the energy parameter  $\varepsilon_{f1}^*$  is shown in figure 8. We also included here the curve for the pre-adsorbed layer of hard obstacles as a reference. As expected, for a low value of  $\varepsilon_{f1}^* = 0.05$ , the evaluated curve  $T_w^*(R_c^*)$  is close to that for hard obstacles. However, we observe an undulated course of this function. The changes in the values of the contact angle result from the changes in the free energies for gaseous and liquid phases contacting with a solid. According to perturbative treatment, the shape of the function  $T_c^*(R_c^*)$  is to a great extent determined by a delicate balance between the hard-sphere contribution to the free energy and the mean-field term due to water-pre-adsorbed molecule attraction. If the latter contribution prevails, the wetting temperature decreases, but when the hard-sphere contribution becomes dominant, the wetting temperature increases.

For  $\varepsilon_{f1}^* = 0.7$ , the wetting temperature decreases and for all values of  $R_c^*$  and for  $R_c^* > 0.4$  this decrease is quite fast. We did not perform the calculations at temperatures lower than  $T_c^* < 1.5$ , because the application of the considered version of the density functional at the temperatures lower than the triple point temperature may be questioned.

Finally, in figure 9 we display the effect of the attractive forces on the structure of gaseous and liquid



**Figure 8.** (Colour online) The dependence of the wetting temperatures on  $R_c^*$  for the system with different values of  $\varepsilon_{f1}^*$  that are given in the figure. The red solid line denotes the results for pre-adsorbed hard-spheres. Calculations are for  $\sigma_1^* = 1$ .

water on modified surfaces. Left-hand panels are at bulk densities marginally lower than the bulk dew density, while right-hand panels are at the bulk liquid density marginally higher than the bulk bubble density. The presence of sites attracting water molecules on the graphite surface greatly influences the structure of both gaseous and liquid adsorbed phases. In the case of adsorption from the gaseous phase, the attraction between pre-adsorbed species and water molecules leads to the formation of a “knee” on the density profile (part a). At higher values of  $R_c^*$ , this knee transforms into the second maximum of  $\rho^*(z)$ . At the highest coverages of the surface with pre-adsorbed molecules, the local density maximum at the value of  $z$  corresponding to a minimum of the potential  $v(z)$  vanishes and the pre-adsorbed layer starts to play the role of the source of an external potential.

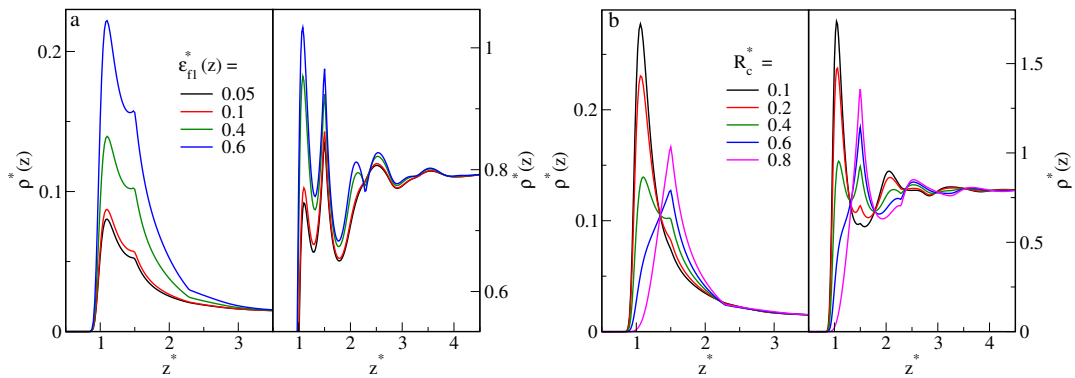


**Figure 9.** (Colour online) Part a. The dependence of local densities of coexisting gaseous (left-hand panel) and liquid (right-hand panel) phases. The calculations were carried out at constant  $R_c^* = 0.4$  and for different values of  $\varepsilon_{f1}^*$  given in the figure. Part b. The same as in part a, but for constant  $\varepsilon_{f1}^* = 0.4$  and for different values of  $R_c^*$ , given in the figure. In all cases  $\sigma_1^* = 1$  and  $T^* = 2$ .

## 4. Summary

We have proposed an approach based on the density functional theory to describe the changes in the contact angle with the surface heterogeneity. According to the proposed model, the surface heterogeneity results from the formation of a layer of pre-adsorbed molecules on the original, bare solid surface. Depending on the model of interactions between the pre-adsorbed molecules, on their size, and on their amount (expressed in terms of the surface density, or surface coverage), different changes in the contact angle and the wetting temperature were observed. In the case of hard-sphere fluid-pre-adsorbed layer interactions, the presence of pre-adsorbed hard-sphere molecules leads to an increase of the values of the contact angle and the wetting temperature. These effects were more pronounced for larger pre-adsorbed particles.

In the case of pre-adsorbed molecules attracting fluid molecules, the changes in the wetting temperature with the amount of pre-adsorbed species are more complex. For some selected values of the parameter characterizing the attractive interaction and for the selected amount of pre-adsorbed molecules, the wetting temperature can exhibit a maximum. Since the value of the wetting temperature depends on the surface excess free energies of gaseous and liquid phases in contact with the modified solid, the presence of a maximum is the result of an interplay between particular terms in the perturbational free energy expansion, basically on the competitions between the hard-sphere and the contribution due to attractive water-pre-adsorbed particles interaction.

The theory considered in this work indicates that the value of the wetting temperature does not depend linearly on the surface density of different kinds of adsorbing sites, as predicted by the classical Cassie approach [37]. Our treatment can also be considered as an alternative to the treatment by Aslyamov et al. [61, 62]. The latter approach is based on the development of an effective, one-dimensional external potential that, in turn, is next used in the classical density functional one-dimensional density functional expressions for evaluating the excess free energy. Instead of evaluating the effective free energy, we propose an appropriate modification of the free energy contributions. Our idea has its origin in an approximate treatment of the quenched-annealed systems that was previously used to study adsorption on heterogeneous surfaces [24–27]. Unfortunately, there exist no experimental or simulation data that would be useful for verifying our theoretical predictions.

Basically, our calculations were carried out for one-component pre-adsorbed phase. However, the theory was proposed for the case of a multicomponent pre-adsorbed layer. It can be also extended to the case of a polydisperse mixture by proceeding along the lines described in [74–76]. Next, the theory can be also extended by assuming a multilayer structure of pre-adsorbed molecules. The treatment of such a system would be based on the approaches used for quenched-annealed systems [11]. All these problems are under study in our laboratories.

## References

1. Sips R., *J. Chem. Phys.*, 1948, **16**, 490, doi:10.1063/1.1746922.
2. Everett D. H., House W. A., In: *Colloid Sciences*, Vol. 4, Everett D. H. (Ed.), The Royal Society of Chemistry, London, 1983, 1–58, doi:10.1039/9781847555861.
3. Bakaev V. A., *Surf. Sci.*, 1988, **198**, 571, doi:10.1016/0039-6028(88)90385-8.
4. Rudzinski W., Everett D. H., *Adsorption of Gases on Heterogeneous Surfaces*, Elsevier Ltd., Amsterdam, 1991.
5. Xia X., Litvinov S., Muhler M., *Langmuir*, 2006, **22**, 8063, doi:10.1021/la061233s.
6. Kumar K. V., Gadipelli S., Wood B., Ramisetty K. A., Stewart A. A., Howard C. A., Brett D. J. L., Rodriguez-Reinoso F., *J. Mater. Chem. A*, 2019, **7**, 10104, doi:10.1039/C9TA00287A.
7. Li H. J., Kang J. H., Pan Z. J., Zhou F. B., Deng J. C., Zhu S. J., *J. Nanosci. Nanotechnol.*, 2021, **21**, 212, doi:10.1166/jnn.2021.18443.
8. Barrow N. J., Brümmer G. W., Strauss R., *Langmuir*, 1993, **9**, 2606, doi:10.1021/la00034a020.
9. Al-Muhtaseb S. A., Ritter J. A., *Langmuir*, 1999, **15**, 7732, doi:10.1021/la990242g.
10. Adamczyk Z., Weroński P., Musiał E., *J. Colloid Interface Sci.*, 2002, **248**, 67, doi:10.1006/jcis.2001.8170.
11. Pizio O., In: *Computational Methods in Surface and Colloid Science*, Ch. 6., Borowko M. (Ed.), CRC Press, New York, 2000.
12. Lafuente L., Cuesta J. A., *Phys. Rev. E*, 2006, **74**, 041502, doi:10.1103/PhysRevE.74.041502.

13. Cheung D. L., Schmidt M., *J. Chem. Phys.*, 2009, **131**, 214705, doi:10.1063/1.3267728.
14. Dong W., Chen X. S., *Sci. China: Phys., Mech. Astron.*, 2018, **61**, 70501, doi:10.1007/s11433-017-9165-y.
15. Pizio O., Patrykiewicz A., Sokołowski S., *J. Phys. Chem. C*, 2007, **111**, 15743, doi:10.1021/jp0736847.
16. Bryk P., Rżysko W., Malijevsky A., Sokołowski S., *J. Colloid Interface Sci.*, 2007, **313**, 41, doi:10.1016/j.jcis.2007.03.077.
17. Lin X., Lu J. C., Shao Y., Zhang Y. Y., Wu X., Pan J. B., Gao L., Zhu S. Y., Qian K., Zhang Y. F., et al., *Nat. Mater.*, 2017, **16**, 717, doi:10.1038/nmat4915.
18. Maurer R. J., Ruiz V. G., Camarillo-Cisneros J., Liu W., Ferri N., Reuter K., Tkatchenko A., *Prog. Surf. Sci.*, 2016, **91**, 72, doi:10.1016/j.progsurf.2016.05.001.
19. Marquetti I., Desai S., *Surfaces*, 2022, **5**, 176, doi:10.3390/surfaces5010010.
20. Centres P. M., Bulnes F., Riccardo J. L., Ramirez-Pastor A. J., Perarnau M. A., *Adsorpt. Sci. Technol.*, 2011, **29**, 613, doi:10.1260/0263-6174.29.7.613.
21. Shi K., Santiso E. E., Gubbins K. E., *Langmuir*, 2020, **36**, 1822, doi:10.1021/acs.langmuir.9b03633.
22. Charmas B., Lebeda R., *J. Chromatogr. A*, 2000, **886**, 133, doi:10.1016/S0021-9673(00)00432-5.
23. Lapčík L., Otyepka M., Otyepková E., Lapčíková B., Gabriel R., Gavenda A., Prudilová B., *Curr. Opin. Colloid Interface Sci.*, 2016, **24**, 64, doi:10.1016/j.cocis.2016.06.010.
24. Chmiel C., Karykowski K., Patrykiewicz A., Rżysko W., Sokołowski S., *Mol. Phys.*, 1994, **81**, 691, doi:10.1080/00268979400100461.
25. Röcken P., Somoza A., Tarazona P., Findenegg G., *J. Chem. Phys.*, 1998, **108**, 8689, doi:10.1063/1.476297.
26. Reszko-Zygmunt J., Pizio O., Rżysko W., Sokołowski S., Sokołowska Z., *J. Colloid Interface Sci.*, 2001, **241**, 169, doi:10.1006/jcis.2001.7721.
27. Rżysko W., Pizio O., Sokołowski S., *J. Mod. Phys.*, 1999, **10**, 891, doi:10.1142/S0129183199000693.
28. Bonn D., Eggers J., Indekeu J., Meunier J., Rolley E., *Rev. Mod. Phys.*, 2009, **81**, 739, doi:10.1103/RevModPhys.81.739.
29. Pizio O., Sokołowski S., *Mol. Phys.*, 2022, **120**, e2011454, doi:10.1080/00268976.2021.2011454.
30. Dietrich S., *Phase Transition and Critical Phenomena*, Vol. 12, Domb C., Lebowitz J. L. (Eds.), Academic Press, London, 1988, 2–218.
31. Dolny K., Evans R., Wills H. H., *Density Functional Theory for Inhomogeneous Fluids I: Simple Fluids in Equilibrium*, Lectures at 3rd Warsaw School of Statistical Physics, University of Bristol, Bristol, UK, 2010.
32. Schick M., In: *Liquids at Interfaces*, Charvolin J., Joanny J. F., Zinn-Justin J. (Eds.), North-Holland, Amsterdam 1990, 415–496.
33. Kaplan W. D., Chatain D., Wynblatt P., Carter W. C., *J. Mater. Sci.*, 2013, **48**, 5681, doi:10.1007/s10853-013-7462-y.
34. Rutledge J. E., Taborek P., *Phys. Rev. Lett.*, 1992, **69**, 937, doi:10.1103/PhysRevLett.69.937.
35. Cassie A. B. D., Baxter S., *Trans. Faraday Soc.*, 1944, **40**, 546, doi:10.1039/TF9444000546.
36. Wenzel R. N., *J. Phys. Chem.*, 1949, **53**, 1466, doi:10.1021/j150474a015.
37. Erbil H. Y., *Colloids Interfaces*, 2021, **5**, 8, doi:10.3390/colloids5010008.
38. Swain P. S., Lipowsky R., *Langmuir*, 1998, **14**, 6772, doi:10.1021/la980602k.
39. Li H., Li A., Zhao Z., Li M., Song Y., *Small Struct.*, 2020, **1**, 2000028, doi:10.1002/ssstr.202000028.
40. Nguyen C. T., Barisik M., Kim B., *AIP Adv.*, 2018, **8**, 065003, doi:10.1063/1.5031133.
41. Zhang B., Wang J., Liu Z., Zhang X., *Sci. Rep.*, 2014, **4**, 5822, doi:10.1038/srep05822.
42. Yatsyshin P., Durán-Olivencia M. A., Kalliadasis S., *J. Phys.: Condens. Matter*, 2018, **30**, 274003, doi:10.1088/1361-648X/aac6fa.
43. Yatsyshin P., Parry A. O., Rascón C., Kalliadasis S., *J. Phys.: Condens. Matter*, 2017, **29**, 094001, doi:10.1088/1361-648X/aa4fd7.
44. Malijevský A., *J. Chem. Phys.*, 2014, **141**, 184703, doi:10.1063/1.4901128.
45. Berim G. O., Ruckenstein E., *J. Colloid Interface Sci.*, 2011 **359**, 304, doi:10.1016/j.jcis.2011.03.037.
46. Ata M. S., Liua Y., Zhitomirsky I., *RSC Adv.*, 2014, **4**, 22716, doi:10.1039/C4RA02218A.
47. Mozetič M., *Materials*, 2019, **12**, 441, doi:10.3390/ma12030441.
48. Nagase K., Kanazawa H., *Anal. Chim. Acta*, 2020, **1138**, 191, doi:10.1016/j.aca.2020.07.075.
49. Jeong S. P., Kumar R., Genix A. C., Popov I., Li C., Mahurin S. M., Hu X., Bras W., Popovs I., Sokolov A. P., Bocharova V., *ACS Appl. Nano Mater.*, 2021, **4**, 5895, doi:10.1021/acsanm.1c00803.
50. Borówko M., Patrykiewicz A., Sokołowski S., Staszewski T., *Collect. Czech. Chem. Commun.*, 2010, **75**, 221, doi:10.1135/cccc2009104.
51. Patrykiewicz A., Sokołowski S., Tscheliessnig R., Fischer J., Pizio O., *J. Phys. Chem. B*, 2008, **112**, 4552, doi:10.1021/jp710978t.
52. Trejos V. M., Sokołowski S., Pizio O., *J. Chem. Phys.*, 2018, **149**, 134701, doi:10.1063/1.5047018.
53. Pizio O., Sokołowski S., *J. Mol. Liq.*, 2022, **357**, 119111, doi:10.1016/j.molliq.2022.119111

54. Patrykiewicz A., Sokołowski S., Pizio O., In: Surface and Interface Science: Solid-Gas Interfaces II, Vol. 6, Wandelt K. (Ed.), Wiley-VCH, 2016, 883–1253, doi:10.1002/9783527680580.ch46.
55. Demerdash O., Wang L. P., Head-Gordon T., WIREs Comput. Mol. Sci., 2018, **8**, e1355, doi:10.1002/wcms.1355.
56. Müller E. A., Gubbins K. E., Ind. Eng. Chem. Res., 2001, **40**, 2193, doi:10.1021/ie000773w.
57. Gubbins K. E., Fluid Phase Equilib., 2016, **416**, 3, doi:10.1016/j.fluid.2015.12.043.
58. Clark G. N. I., Haslam A. J., Galindo A., Jackson G., Mol. Phys., 2006, **104**, 3561, doi:10.1080/00268970601081475.
59. Gloor G. J., Jackson G., Blas F. J., del Río E. M., de Miguel E., J. Chem. Phys., 2004, **121**, 12740, doi:10.1063/1.1807833.
60. Steele W. A., The Interaction of Gases with Solid Surfaces, Pergamon Press, Oxford, 1974.
61. Aslyamov T., Khlyupin A., Pletneva V., Akhatov I., J. Phys. Chem. C, 2019, **123**, 28707, doi:10.1021/acs.jpcc.9b07761.
62. Aslyamov T., Pletneva V., Khlyupin A., J. Chem. Phys., 2019, **150**, 054703, doi:10.1063/1.5079708.
63. Zhou S., J. Stat. Phys., 2018, **170**, 979, doi:10.1007/s10955-018-1968-2.
64. Jackson G., Chapman W. G., Gubbins K. E., Mol. Phys., 1988, **65**, 1, doi:10.1080/00268978800100821.
65. Chapman W. G., Jackson G., Gubbins K. E., Mol. Phys., 1988, **65**, 1057, doi:10.1080/00268978800101601.
66. Vallejos-Burgos F., Ohba T., Kaneko K., In: Nanoporous Materials for Gas Storage, Kaneko K., Rodríguez-Reinoso F. (Eds.), Springer, Singapore, 2019, doi:10.1007/978-981-13-3504-4\_2.
67. Zhao X., Johnson J. K., Mol. Simul., 2005, **31**, 1, doi:10.1080/0892702042000272889.
68. Yu Y. X., Wu J., J. Chem. Phys., 2002, **117**, 10156, doi:10.1063/1.1520530.
69. Trejos V. M., Sokołowski S., Pizio O., Mol. Phys., 2020, **118**, 1615647, doi:10.1080/00268976.2019.1615647.
70. Edelmann M., Roth R., J. Chem. Phys., 2016, **144**, 074105, doi:10.1063/1.4942020.
71. Jasper W. J., Anand N., J. Mol. Liq., 2019, **281**, 196, doi:10.1016/j.molliq.2019.02.039.
72. Bryk P., Bucior K., Sokołowski S., Żukociński G., J. Phys.: Condens. Matter, 2004, **16**, 8861, doi:10.1088/0953-8984/16/49/005.
73. Trejos V. M., Pizio O., Sokołowski S., Fluid Phase Equilib., 2018, **473**, 145, doi:10.1016/j.fluid.2018.06.005.
74. Pizio O., Patrykiewicz A., Sokołowski S., Mol. Phys., 2001, **99**, 57, doi:10.1080/00268970010000980.
75. Jorge S., Schöll-Paschinger E., Kahl G., Fernaud J. M., Mol. Phys., 2003, **101**, 1733, doi:10.1080/0026897031000085128.
76. Yu Y. X., Wu J., Xin Y. X., Gao G. H., J. Chem. Phys., 2004, **121**, 1535, doi:10.1063/1.1763142.

## Кут змочування води на модельній гетерогенній поверхні. Метод функціоналу густини

К. Домбровська<sup>1</sup>, О. Пізіо<sup>2</sup>, С. Соколовський<sup>1</sup>

<sup>1</sup> Факультет теоретичної хімії, Університет ім. Марії Склодовської-Кюрі, Люблін 20-031, Польща,  
email: stefan.sokolowski@gmail.com

<sup>2</sup> Інститут хімії, Національний автономний університет Мехіко, Circuito Exterior, 04510, Мехіко, Мексика  
email: oapizio@gmail.com

За допомогою методу функціоналу густини розраховано кут змочування у моделі води на гетерогенній графітоподібній поверхні. Неоднорідність поверхні створена шаром преадсорбованих сферичних частинок, або ж сумішшю молекул різних розмірів. Наявність преадсорбованого шару призводить до виникнення геометричної та енергетичної гетерогенності поверхонь. Розглянуто два випадки. Преадсорбовані молекули можуть або поводити себе як перешкоди у вигляді твердих сфер, або можуть також притягувати до себе молекули води. У першому випадку збільшення кількості преадсорбованих складників призводить до зростання температури змочування, яке, однак, не залежить лінійно від кількості перешкод. У тому випадку, коли перешкоди притягують молекули води, криві, що описують залежність кута змочування від кількості преадсорбованих частинок, можуть мати максимум. Крім того, було досліджено, яким чином преадсорбовані складники суміші впливають на локальні густини газоподібних і рідких фаз при їх контакті з модифікованою твердою поверхнею.

**Ключові слова:** метод функціоналу густини, кут змочування, неоднорідна поверхня, модель води

---

---